Ceramics International xxx (xxxx) xxx–xxx

Contents lists available at ScienceDirect

Ceramics International

journal homepage: www.elsevier.com/locate/ceramint

Study on the mechanical properties of porous tin oxide

Kyungju Nam[a], Jeff Wolfenstine[b], Hyelim Choi[a], Regina Garcia-Mendez[c], Jeff Sakamoto[d], Heeman Choe[a,*]

[a] School of Materials Science and Engineering, Kookmin University, 77 Jeongneung-ro, Seongbuk-gu, Seoul 02707, Republic of Korea
[b] Army Research Laboratory, RDRL-SED-C, 2800 Powder Mill Road, Adelphi, MD 20783, USA
[c] Department of Materials Science and Engineering, University of Michigan, Ann Arbor, MI 48109, USA
[d] Department of Mechanical Engineering, University of Michigan, Ann Arbor, MI 48109, USA

ARTICLE INFO

Keywords:
C. Mechanical properties
A. sintering
B. porosity
E. sensors
Tin oxide

ABSTRACT

Despite the importance of tin oxide (SnO_2) in diverse functional applications, little information is available on the mechanical properties of bulk or porous SnO_2. In this study, porous SnO_2 was synthesized using an ice-templating method to produce a "dual" pore structure that comprises large wall pores (on the order of several micrometers) with small micropores (~2 μm) on their surfaces. The Vickers hardness decreased with increasing porosity and increased with increasing contiguity of struts. The compressive stress–strain curves of porous SnO_2 samples with porosity ranging from 48% to 73% were compared with both the Gibson–Ashby and the cellular-lattice-structure-in-square-orientation models, which generally represent the "lower" and "upper" bounds of yield strength for porous materials, respectively. As expected, the yield strength of the porous SnO_2 samples decreased with increasing porosity, and all the yield-strength values of porous SnO_2 fell between the two extreme prediction models. The sample with the lowest porosity of 48% exhibited sharply increasing elastic behavior followed by sudden rupture, as generally reported for bulk ceramics; however, the other samples with higher porosities ranging from 50% to 73% exhibited "porous-metal-like" behavior at strains of 15% or greater as a result of the fracturing of the solid walls between the pores.

1. Introduction

In the past few decades, porous ceramics have attracted increasing attention in numerous functional applications such as filtration [1], energy production [2], biomaterials [3,4], and gas sensors [5]. Among these porous ceramics, porous tin oxide (SnO_2) is one of the most well-known and popular functional materials because of its diverse excellent properties; *e.g.*, it is used in gas sensors as a semiconductor [5,6], in lithium (Li)-ion battery electrodes as an electrochemically active material [7], and in solar cells [8] and light-emitting diodes (usually in the form of indium tin oxide) as a semiconductor [9–11]. Surprisingly, despite the significant importance of SnO_2 in these diverse functional applications, no systematic study on the mechanical properties of bulk or porous SnO_2 has been reported.

Even in cases where porous SnO_2 is used in functional applications, a good understanding of its mechanical properties is important because sufficient mechanical reliability is still required. With increasing porosity (increased surface area for improved electrochemical efficiency), the mechanical properties of porous SnO_2 should degrade. On the other hand, with decreasing porosity the mechanical reliability under load-bearing conditions increases, with a concurrent decrease in the surface area leading to reduced electrochemical efficiency. Therefore, an optimized combination of porosity and mechanical integrity of porous SnO_2 should be achieved depending on its application. This goal is even more difficult to achieve given that in most cases, porous SnO_2 is used in the form of a thin film for functional applications [9,11]; this makes it more prone to a premature mechanical failure.

To this end, a thorough evaluation of the mechanical properties of porous SnO_2 is indispensable. This paper reports on the physical and mechanical properties of porous SnO_2. We synthesize porous SnO_2 via an ice-templating method to carefully design the pore size, density, orientation, and shape by controlling the starting powder content, solidification speed and direction, and sintering time and temperature. The final synthesized SnO_2 structure is a "dual" pore structure that consists of large pores between the walls and small micropores on the surface of the walls [5]. In the present paper, strut size and contiguity are also analyzed quantitatively on the basis of the common grain growth theory [12] and Fan's approach [13], respectively. Furthermore, we characterize the mechanical properties (hardness, yield strength) of

* Corresponding author.
E-mail address: heeman@kookmin.ac.kr (H. Choe).

http://dx.doi.org/10.1016/j.ceramint.2017.05.128
Received 14 April 2017; Received in revised form 12 May 2017; Accepted 16 May 2017
0272-8842/ © 2017 Elsevier Ltd and Techna Group S.r.l. All rights reserved.

porous SnO_2 using both Vickers hardness and compressive tests as a function of porosity. In addition, the compressive yield strength as a function of porosity is compared with the predictions based on the Gibson–Ashby [14] and simplified compressive models [15,16].

2. Experimental procedures

2.1. Sample preparation

We synthesized porous SnO_2 via an ice-templating method. An SnO_2 powder slurry was created by mixing 44 wt% nanosized SnO_2 powder (with a mean particle size of ~80 nm, 99.9% purity, Inframat Advanced Materials, USA), 3 wt% polyvinyl alcohol (PVA, Sigma-Aldrich Co., USA) as a binder and 0.5 wt% nanosized CuO powder (with a mean particle size of 40–80 nm, 99.9% purity, Inframat Advanced Materials, USA) as sintering agent in a solution of deionized water as reported previous study [5]. The prepared SnO_2 slurry was then poured into a cylindrical mold (43 mm and 56 mm inner and outer diameters, respectively, and a height of 70 mm) consisting of insulated Teflon walls on a Cu rod, which was cooled using liquid nitrogen. The temperature of the Cu rod was controlled using a thermocouple and temperature controller. After the freezing process was complete, the frozen SnO_2–ice sample was removed from the mold and dried at 80 °C for 48 h in a freeze dryer (FDU–7003, Operon, Republic of Korea) under a 10^{-2} Torr residual pressure. This produced a SnO_2 green body with directional pores. The resulting porous green-body sample was then heat-treated in two separate steps. It was first subjected to a pre-heat treatment at 300 °C for 3 h to remove the binder before being sintered at an elevated temperature in a box furnace under atmospheric air; with sintering temperatures of 1050, 1100, 1150 and 1250 °C for up to 10 h with heating and cooling rates of 5 °C min^{-1} and 3 °C min^{-1}, respectively. The density of the porous SnO_2 samples was determined by measuring the mass and physical dimensions of parallelepiped samples that were machined to precise dimensions. For comparison, ~~the~~ SnO_2 powders were consolidated by hot-pressing to synthesize dense SnO_2 samples. The SnO_2 powders were loaded into a graphite die and heated at 500 °C under 395 MPa of pressure for 1 h. The relative density of this sample was 99.3 ± 0.4%.

2.2. Physical and mechanical characterization

The microstructure was characterized by scanning electron microscopy (SEM, JSM7401F, JEOL, Japan). We carried out X-ray diffraction (XRD, DMAX2500, Rigaku, Japan) tests on selected porous SnO_2 samples to examine changes in phase and crystallite size from the initial SnO_2 powder to the final porous SnO_2 samples. We also assessed the porous SnO_2 sample's contiguity, which represents the degree of strut connectivity, using Fan's approach [13]. We attempted to minimize any probable cause of error by drawing more than ten random lines of unit length on each examined micrograph and by carefully conducting intercept measurements according to ASTM standards [17].

Vickers hardness testing was performed over the load range of 98–490 mN using a micro-Vickers tester (810–352 K, Mitutoyo, Japan). The indent impression was measured after an indent time of ~10 s. Uniaxial compressive tests (Z020, Zwick GmbH & Co., Germany) were performed on parallelepiped porous SnO_2 samples with dimensions of 3.0 mm×3.0 mm ×6.0 mm at a nominal strain rate of 0.0001 s^{-1} with their longitudinal axis parallel to the compressive loading direction.

3. Results and discussion

3.1. Processing and morphology

Fig. 1 compares the XRD patterns of the initial SnO_2 powder and the porous SnO_2 heat-treated at 1250 °C for 10 h. From Fig. 1 no noticeable difference between the two XRD patterns is observed and when compared to the pure SnO_2 reference, it is seen that both samples consist only of single phase SnO_2. On the other hand, the mean crystallite size of the powder and the porous SnO_2, which was calculated using the Scherrer equation, increases from 47 nm to 71 nm after the heat-treatment at 1250 °C.

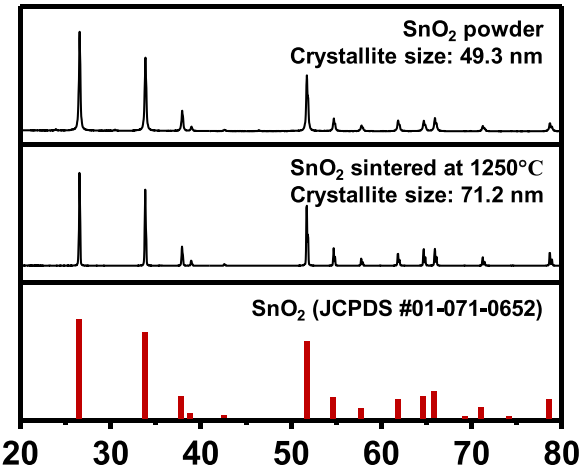

Fig. 1. XRD patterns of the initial SnO_2 powder and the porous SnO_2 heat-treated at 1250 °C for 10 h.

Fig. 2 shows SEM images of porous SnO_2 synthesized via the ice-templating process and sintered at 1050–1250 °C. Fig. 2(a) shows the fractured surface morphology of the lamellar pores created by the ice dendrites during freezing. Fig. 2(b) shows the top-view surface morphology, perpendicular to the freezing direction. From the cross-sectional images shown in Fig. 2(c)–(e) of samples sintered at 1050 °C, 1150 °C, and 1250 °C, respectively, the mean width of the elongated wall struts are measured. As expected, the mean width of the elongated walls increases from 1.9 to 3.9 μm as the sintering temperature increases from 1050 to 1250 °C. The aligned, lamellar macropores with similar dimensions are uniformly surrounded by parallel SnO_2 walls with very small micropores (~2 μm) on their surfaces. This dual pore structure is attributed to the inherent nature of ice-crystal growth, where the ice growth velocity in the direction parallel to the direction of the temperature gradient is greater than that in the direction perpendicular to the gradient [18–20].

The strut size gradually increases with the sintering temperature because more SnO_2 struts tend to connect together into larger struts, as shown in Fig. 2. Despite the importance of strut size and morphology on the mechanical properties of porous materials, no theory has been proposed to describe the strut growth mechanism. On the basis of previous literature results [5] describing the relationship between the mean grain size and the sintering time and temperature, the mean strut size can also be expressed in terms of sintering time and temperature, as shown below in Eq. (1). The relationship between the mean strut size and the sintering temperature of porous SnO_2 in this study is expected to follow the relationship between the mean grain size and sintering temperature under the assumption that the two phenomena have the same fundamental growth mechanism.

The relationship between the mean strut size and sintering temperature of porous SnO_2 is described as follows [5,12,21]:

$$D^3 - D_0^3 = K_0 t \exp\left(-\frac{Q}{RT}\right) \quad (1)$$

where D is the mean strut size for a certain sintering condition from the initial mean strut size D_0 (0.49 μm), Q is the activation energy (37.3 kJ/mol, calculated from the slope of the line in Fig. 3), and K_0 is a proportionality constant that can be determined experimentally. Here, all the samples were sintered for the same duration (10 h) at various sintering temperatures ranging from 1050 °C to 1250 °C. The

Download English Version:

https://daneshyari.com/en/article/5438035

Download Persian Version:

https://daneshyari.com/article/5438035

Daneshyari.com